RSC Advances

PAPER

View Article Online
View Journal | View Issue

Cite this: *RSC Adv.*, 2017, **7**, 45885

Facile synthesis of visible-light-driven $Cu_2O/BiVO_4$ composites for the photomineralization of recalcitrant pesticides†

E. Aguilera-Ruiz,[a] M. de la Garza-Galván,[a] P. Zambrano-Robledo,[a] J. C. Ballesteros-Pacheco,[b] J. Vazquez-Arenas,[c] J. Peral[d] and U. M. García-Pérez*[a]

Received 1st August 2017
Accepted 20th September 2017

DOI: 10.1039/c7ra08513c

rsc.li/rsc-advances

$Cu_2O/BiVO_4$ composites with different Cu_2O co-catalysts were synthesized by a simple impregnation method at 200 °C for 4 h under N_2 atmosphere. The Cu_2O powder was obtained through the chemical reduction of copper sulfate using different reducing reagents such as ascorbic acid, glucose or fructose. The as-synthesized samples were characterized by X-ray powder diffraction, scanning and transmission electron microscopies, UV-vis diffuse reflection absorption and electrochemical impedance spectroscopy. The photoactivities of the $Cu_2O/BiVO_4$ composites were evaluated in terms of the mineralization of 4-chlorophenol (4-CP) in aqueous solutions under visible-light irradiation. The role of experimental variables including the preparation method of the co-catalyst, catalyst concentration, and 4-chlorophenol initial concentration in the photocatalytic performance of $Cu_2O/BiVO_4$ catalysts was analyzed. Likewise, the viability to recover and reuse these photocatalysts was also tested. It was found that the complete abatement of 4-CP led to the formation of chlorocatechol (4-CC) without concomitantly involving the formation pathway of hydroquinone/*p*-benzoquinone, 4-CC was identified in the light of experimental evidence (UV-vis) and spectral simulation done by using time-dependent density functional theory (TD-DFT) with the polarized continuum model.

1. Introduction

Nowadays, the generation of wastewater from industries and households is one of the largest environmental problems that modern society needs to address, since clean water is a non-renewable resource essential to human life.[1] Chlorophenols are among the most dangerous pollutants to remove from water due to their high biorecalcitrant character, even at low concentrations, being extremely dangerous to living organisms. These compounds are used in different applications including additives for wood, paint and vegetable fiber preservation, or as disinfectants.[2] For example, 4-chlorophenol, is used in the synthesis of quinizarin (dye), clofibrate (drug), chlorophenesin and dichlorophen (fungicides).[1]

An extensive amount of research has been carried out in order to remove numerous compounds of this family by using different strategies which include physical, biological, and chemical methods, like absorption onto activated carbon, microbial degradation and advanced oxidation processes (AOPs), respectively.[3] The use of AOPs in the abatement of recalcitrant pollutants has been widely known for years, having the advantages of a potential complete mineralization of organic pollutants to CO_2 achieved under mild conditions. One of the most efficient AOPs is heterogeneous photocatalysis with semiconductor materials.

Since the pioneering work of Fujishima and Honda, back in 1972, TiO_2 has been the most used and studied photocatalyst.[4–7] Nevertheless, the research about heterogeneous photocatalysis with other materials has been increasing during the last years; with the goal of developing new catalytic materials that could be activated by visible-light irradiation, either through metal or non-metal doping, surface sensitization, semiconductor coupling, noble metal deposition, or crystal defect increase.[8]

Two of those novel semiconductors are cuprous oxide (Cu_2O) and bismuth vanadate ($BiVO_4$), materials that have been widely studied mainly because their absorption maxima are in the visible region of the electromagnetic spectrum. Cu_2O is a p-type

[a]*Universidad Autónoma de Nuevo León, Facultad de Ingeniería Mecánica y Eléctrica, Centro de Investigación e Innovación en Ingeniería Aeronáutica, Carretera a Salinas Victoria Km 2.3, C. P. 66600, Apodaca, Nuevo León, Mexico. E-mail: ulisesma.garcia@gmail.com; Fax: +52 81 83 32 09 03; Tel: +52 81 83 29 40 20*

[b]*Universidad Politécnica de Lázaro Cárdenas, Departamento de Ingeniería Ambiental, Laboratorio de Sustentabilidad Energética, Av. Galeana S/N, Col. 600 Casas, C. P. 60950, Lázaro Cárdenas Michoacán, Mexico*

[c]*Centro Mexicano para la Producción más Limpia, Instituto Politécnico Nacional, Av. Acueducto s/n, Col. La Laguna Ticomán, Ciudad de México, 07340, Mexico*

[d]*Universitat Autònoma de Barcelona, Department de Química, 08193 Cerdanyola del Vallès, Spain*

† Electronic supplementary information (ESI) available. See DOI: 10.1039/c7ra08513c

semiconductor with direct band gap between 2.0 and 2.2 eV,[9,10] and its use has increased in the recent years due to its low toxicity, good photon absorption and photoelectrochemical hydrogen production from water splitting. This material can be obtained by different synthesis routes, such as chemical reduction, microwave-assisted precipitation method, hydrothermal method and chemical oxidation.[9–14] On the other hand, $BiVO_4$ is a n-type semiconductor with direct band gap of 2.4 eV (monoclinic phase), that presents good chemical stability and photocatalytic properties.[15] This material has been extensively considered as binary and ternary heterostructured photocatalyst for the abatement of recalcitrant compounds due to its adequate crystallinity and narrow band gap.[16–18] To this concern, Guo *et al.* fabricated $BiVO_4$/$InVO_4$ heterojunctions for the degradation of rhodamine B highlighting that the enhanced photocatalytic activity of this composite was due to the combined effect created by two different semiconductors.[17] In the same direction, Lin *et al.* also synthesized ternary heterostructured Ag–$BiVO_4$/$InVO_4$ composite which displayed considerable photocatalytic activity for 4-CP degradation compared to single and binary photocatalysts. This synergism was assigned to the strong absorption in the visible region resulting from Ag nanoparticles incorporation, and the low recombination rate of the electron–hole pairs due to the heterostructured combination of Ag, $BiVO_4$ and $InVO_4$.[18]

It is well known that the main process in heterogeneous photocatalysis is the generation of the electron–hole pair. Those charge carriers are able to react with electron donors and acceptors that approach the catalyst surface. However, those charges could recombine and dissipate the energy, and many research efforts have focused on the reduction of the rate of the recombination processes by using heterojunctions of semiconductors within the frame of a composite.[19,20] For example, Cu_2O/$BiVO_4$ composite p–n heterojunction has shown enhanced visible-light photoactivity for the reduction of inorganic and organic compounds, such as carcinogens (Cr(VI)), dyes (methylene blue, methyl orange, crystal violet and rhodamine B) and alcohols (phenol).[21–25] Wang *et al.* evaluated the photoactivity for methylene blue degradation, where the interaction between Cu_2O and $BiVO_4$ materials narrowed the bandgap of $BiVO_4$ to incentive the charge transfer across the interface and spreading the absorption range of visible-light.[21] Yuan *et al.* described the preparation of Cu_2O/$BiVO_4$ composites to eliminate methylene blue and other anionic and cationic dyes (rhodamine B, crystal violet, methyl orange) under visible-light irradiation. An enhanced photocatalytic activity was revealed when Cu_2O was incorporated in the optimal 2.5 mol percentage, since it successfully mitigated the recombination of photogenerated electrons and holes, compared to single Cu_2O or $BiVO_4$ materials.[23]

Under this premise and to the best of our knowledge, most studies conducted with this binary composite have focused on eliminating dyes while, no prior study has undertaken the photodegradation of a colorless organochlorine compound (4-chlorophenol) in aqueous solution using Cu_2O/$BiVO_4$ composite as catalyst. It is evident that this information is critical to figure out the degradation of other chemical structures using this composite, and extending its applicability towards other contaminants.

In this research, Cu_2O/$BiVO_4$ composites with different Cu_2O co-catalysts were synthesized by a simple impregnation method, and their photoactivities were assessed in terms of the degradation of 4-chlorophenol under visible-light irradiation for the first time. The influence of different experimental conditions (4-CP initial concentration, photocatalyst concentration and O_2 flux) towards the photomineralization of this organic compound has been investigated in detail. Multiple 4-chlorophenol by-products are detected during the treatment using experimental and computed simulated UV-vis spectra, the last obtained by applying time-dependent density functional theory, and subsequently contrasted with spectra found in the literature.

The reusability of the catalyst was also studied, and a correlation is established between its performance and its structural, optical and electrochemical properties.

2. Experimental

2.1 Synthesis of semiconductors

Cu_2O powders were synthesized through the chemical reduction of copper sulfate using three different reducing agents: glucose, fructose or ascorbic acid.

In a typical procedure, 0.0349 mol of $CuSO_4 \cdot 5H_2O$ were dissolved in 50 mL of distilled water. Subsequently, 0.07 mol of NaOH and 0.035 mol of sodium–potassium tartrate were dissolved in 50 mL of distilled water, and this solution was poured into the copper solution under continuous stirring. Then, 50 mL of the reducing agent aqueous solution (0.7 M of ascorbic acid and 1.4 M of fructose or glucose) were prepared and added into the copper–tartrate basic solution, forming a colored precipitate. The pH of all suspensions was adjusted to 10. The color of the precipitate changed depending on the reducing agent; red for glucose, orange for fructose and yellow for ascorbic acid. The resulting powders were separated by filtration, washed with distilled water and dried with acetone. The samples synthesized by using ascorbic acid, fructose or glucose as reducing agent were named as Cu_2O–A, Cu_2O–F and Cu_2O–G, respectively. The different synthesis conditions for each method are shown in Table 1.

$BiVO_4$ powder was synthesized by co-precipitation method using sodium carboxymethylcellulose (CMC) as template-structuring agent following the procedure previously described by our group.[26] The final precursor suspension was heated to eliminate the solvents and the resulting powder thermally treated at 350 °C for 24 h.

Table 1 Synthesis parameters of semiconductors

Reducing reagent	NaOH/tartrate (mol)	Temperature (°C)	pH
Ascorbic acid	0.07/0.035	25	10
Fructose	0.105/0.05	60	12
Glucose	0.105/0.05	60	11

2.2 Synthesis of $Cu_2O/BiVO_4$ composites

The $Cu_2O/BiVO_4$ composite powders were prepared by the impregnation method previously reported by our group.[24] In a typical procedure: 2 g of $BiVO_4$ and 0.02 g of Cu_2O powders were mixed mechanically in agate mortar. Such amount of Cu_2O corresponds to a weight ratio of 1%. Then, the resultant mix was submitted to a thermal treatment at 200 °C for 4 h under nitrogen atmosphere, in order to obtain the $Cu_2O/BiVO_4$ composite photocatalysts. These materials synthesized using Cu_2O–A, Cu_2O–F or Cu_2O–G powders as co-catalyst were named as $Cu_2O/BiVO_4$–A, $Cu_2O/BiVO_4$–F and $Cu_2O/BiVO_4$–G, respectively.

2.3 Characterization of photocatalysts

The structural properties of as-synthesized powders were investigated by X-ray powder diffraction (XRD, PANalytical Empyrean) with Cu Kα ($\lambda = 1.5417$ Å) as radiation source. The morphology was investigated by scanning and transmission electron microscopies (SEM, JEOL JSM-6510LV and TEM, JEOL 1400). The optical properties were measured using a diffuse reflectance UV-vis spectrophotometer (DRS, Shimadzu UV-2600) and the absorption spectra were obtained by using $BaSO_4$ as reference. The electrochemistry measurements were collected using a potentiostat/galvanostat Autolab PGSTAT302N.

2.4 Preparation of photocatalyst films

All photocatalyst films were prepared by dip-coating process. Deposition was performed on fluorine-doped tin oxide (FTO) glass (1 cm^2). In a typical process, 30 mg of the photocatalyst were dispersed in 10 mL of ethanol. After that, the suspension was put in ultrasonic bath for 5 min to eliminate aggregates. Then, the substrate was sequentially immersed in the suspension at room temperature for 200 cycles using an immersion speed of 0.25 mm s^{-1}. Electrochemical impedance spectroscopy (EIS) of the catalyst films deposited onto the FTO glass was carried out under potentiostatic mode (wave amplitude of 10 mV) using a standard three-electrode cell with Ag/AgCl (3.0 M KCl) and a platinum rod as reference electrode and counter-electrode, respectively. The electrolyte was a 0.5 M Na_2SO_4 aqueous solution.

The flat-band potentials (E_{fb}) of the semiconductors were calculated by extrapolation to the x-axis of plots of $1/C^2$ *vs.* potential (V). The potentials were referenced to the normal hydrogen electrode (NHE) using the following equation:

$$E_{fb} = E_{ext} + E^0_{Ag/AgCl} + 0.059pH \quad (1)$$

where $E^0_{Ag/AgCl}$ (3.0 M KCl) = 0.209 V *vs.* NHE at 25 °C and E_{ext} is the extrapolated potential to the x-axis.

2.5 Photocatalytic reactions

The photoactivities of the samples were tested using the 4-chlorophenol degradation in a double wall cylindrical photochemical reactor made of borosilicate glass that was kept at 25 °C. The visible-light source of the experiments was a 54 W LED lamp built with blue, green and yellow LEDs of high power (3 W). The radiant flux of visible LED-lamp was 3.56×10^{16} photons per s per cm^2, and was measured using Reinecke's salt as chemical actinometer.[24] The emission spectrum and an image of the lamp are shown in the Fig. S1 (ESI†).

The photocatalytic experiments were carried out by adding 1 g L^{-1} of the photocatalyst to 250 mL of a 4-CP solution with an initial total organic carbon (TOC) concentration of 50 mg L^{-1}. After that, the suspension was put in an ultrasonic bath for 3 min to eliminate aggregates. The solution was kept in the dark for 1 h in order to ensure that adsorption–desorption equilibrium of the pesticide on the photocatalyst surface was reached. After that, the light source was turned on. During the reaction, samples of 9 mL were withdrawn at fixed time intervals and then separated by double centrifugation. The TOC content was measured using a Shimadzu TOC-L analyzer.

The effect of the 4-CP initial concentration was studied, and the concentrations tested were 50, 100, and 200 mg L^{-1}. The effect of the photocatalysts concentration was also studied, and the experiments were carried out with 1, 3 and 5 g L^{-1} of catalyst; another studied factor was the presence of continuous O_2 flux during the photomineralization of 4-CP. Finally, the reuse of the material was tested by using the same material in three consecutive runs.

Hydroquinone (HQ) was purchased from Sigma-Aldrich (≥99%), and used as received without further purification as standard for its potential detection as intermediate during 4-CP photodegradation. A 50 mg L^{-1} aqueous solution was prepared to characterize its UV-vis spectrum.

2.6 Theoretical methods

Calculations were computed in the framework of the density functional theory (DFT). The optimized structures (*i.e.* fundamental states of 4-CP) and frequency analyses were performed using the B3LYP hybrid density functional.[27] UV-vis spectra were computed using a time-dependent density functional theory (TD-DFT) with the polarized continuum model (PCM),[28] using the dielectric constant for water. All calculations were conducted using the 6-311+g(d,p) basis set (split-valence triple-zeta with polarized and diffuse functions), as implemented in Gaussian 09, Revision D.01 software.

3. Results and discussions

3.1 Synthesis of semiconductors

The synthesis of the Cu_2O co-catalyst using different reducing agents and potassium sodium tartrate as chelating agent lead to the formation of powders with different colors, indicating that their optical properties and particle sizes are different.[29] The chemical reactions occurring during the synthesis are described below.

The synthesis of Cu_2O in presence of glucose (reducing agent) can occur through the reaction of Cu^{2+} ions and potassium sodium tartrate in alkaline aqueous media to obtain the bis(tartrato)cuprate(II) complex (reactions (2) and (3)). Subsequently, this reacts with glucose in alkaline media, oxidizing the

aldehyde group contained in the sugar to carboxylic acid and reducing the Cu^{2+} ions to Cu^{+} to produce a red precipitate of Cu_2O (reaction (4)).

$$CuSO_4 + H_2O \rightarrow Cu^{2+}{}_{(aq.)} + SO_4{}^{2-}{}_{(aq.)} \quad (2)$$

The use of potassium sodium tartrate in the synthesis of Cu_2O avoided the reaction between Cu^{2+} and ^{-}OH ions to form $Cu(OH)_2$ (reaction (7)), which is an undesirable product because it can dissociate into CuO in basic aqueous solutions (reaction (8)).[31]

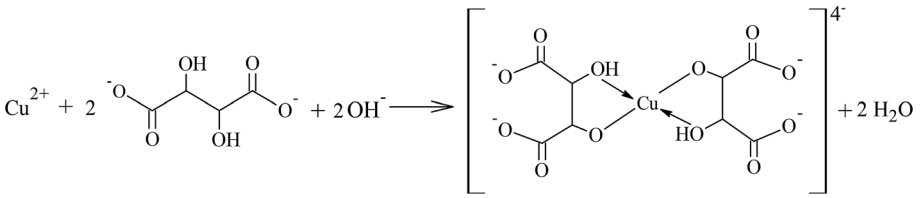

(3)

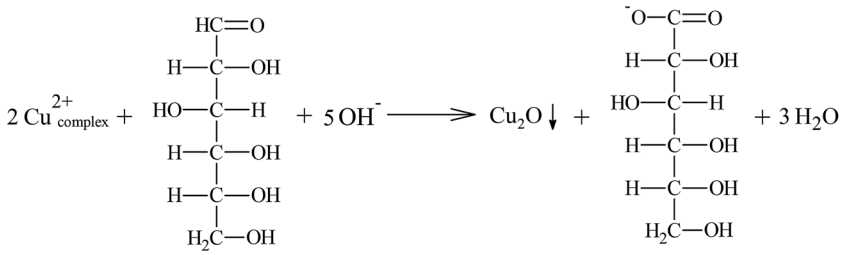

(4)

Cu_2O precipitation using fructose (reducing agent) can be explained according to the Lobry de Bruyn–van Ekenstein Alberda transformation (LDB–AvE),[30] where fructose is isomerized in a basic medium to a mixture of aldoses (glucose and mannose) *via* a tautomeric enediol intermediate (reaction (5)). Then, the reaction (4) takes place forming an orange Cu_2O precipitate.

$$Cu^{2+} + 2OH^{-} \rightarrow Cu(OH)_2 \quad (7)$$

$$Cu(OH)_2 \rightarrow CuO + H_2O \quad (8)$$

3.2 Structural characterization

Fig. 1 shows the XRD patterns of the as-synthesized Cu_2O using different reducing reagents. The characteristic diffraction peaks

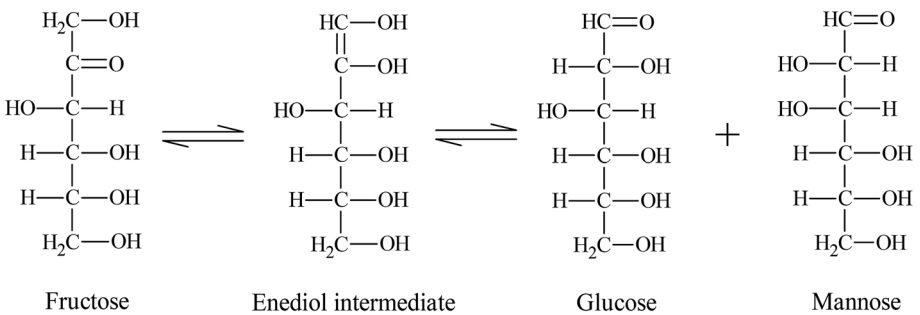

(5)

Cu_2O formation using ascorbic acid (reducing agent) occurs through the oxidation of the ascorbic acid enediol group into a diketone to produce dehydroascorbic acid, thereby reducing the Cu^{2+} to Cu^{+} with the formation of a yellow Cu_2O precipitate, as shown in reaction (6).

of the cubic phase were observed at $2\theta = 29.55$, 36.41, 42.29 and 61.34° (JCPDS card no. 65-3288), which correspond to the crystal planes (110), (111), (200) and (220) of crystalline Cu_2O, respectively. No other diffraction peaks were detected for impurities such as Cu or CuO. The crystallite size of the Cu_2O powders was

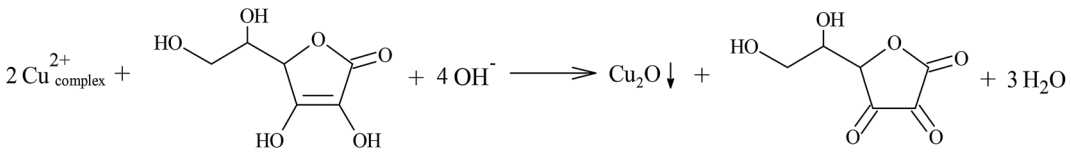

(6)

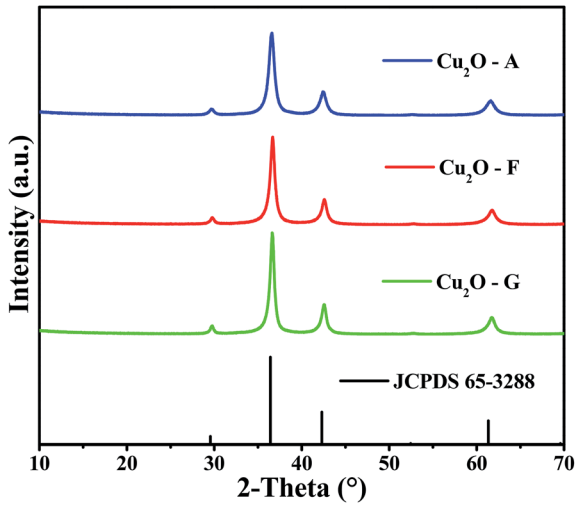

Fig. 1 XRD patterns of the as-synthesized Cu_2O powders using different reducing reagents.

calculated according to Debye–Scherrer equation from the full width at half maximum height of the diffraction peaks.[32] The crystallite size values were 9, 11 and 13 nm for the as-synthesized Cu_2O–A, Cu_2O–F and Cu_2O–G, respectively.

XRD patterns of the as-prepared $BiVO_4$ and $Cu_2O/BiVO_4$ composites are shown in Fig. S2.† The observed $BiVO_4$ diffraction peaks can be associated with the monoclinic phase (JCPDS card no. 14-0688) at $2\theta = 18.67$, 18.98, 28.8, 28.95, 30.52, 34.49, 35.21, and 39.77°. These diffraction peaks indicated that the impregnation of 1 wt% of Cu_2O did not make any change in the monoclinic crystal structure of the $BiVO_4$. Likewise, no diffraction peak of the oxide was observed in the composite XRD patterns, presumably due to its low concentration.

3.3 Morphological characterization

Fig. 2 shows the SEM images of the $Cu_2O/BiVO_4$ composites synthesized by impregnation method at 200 °C for 4 h under N_2 atmosphere, and using Cu_2O–F, Cu_2O–G and Cu_2O–A as co-catalyst. All the composites exhibited morphologies very similar to that of pure $BiVO_4$. Meanwhile, the pure Cu_2O particles showed spherical morphology with different particle sizes depending on the reducing agent. The particle size decreased in the following order: Cu_2O–G > Cu_2O–F > Cu_2O–A.

Fig. 2c shows that the Cu_2O–A composite presents a quasi-spherical morphology similar to pure $BiVO_4$, where it was not possible to differentiate between both morphologies due to the nanometric quasi-spherical shape of pure Cu_2O–A.

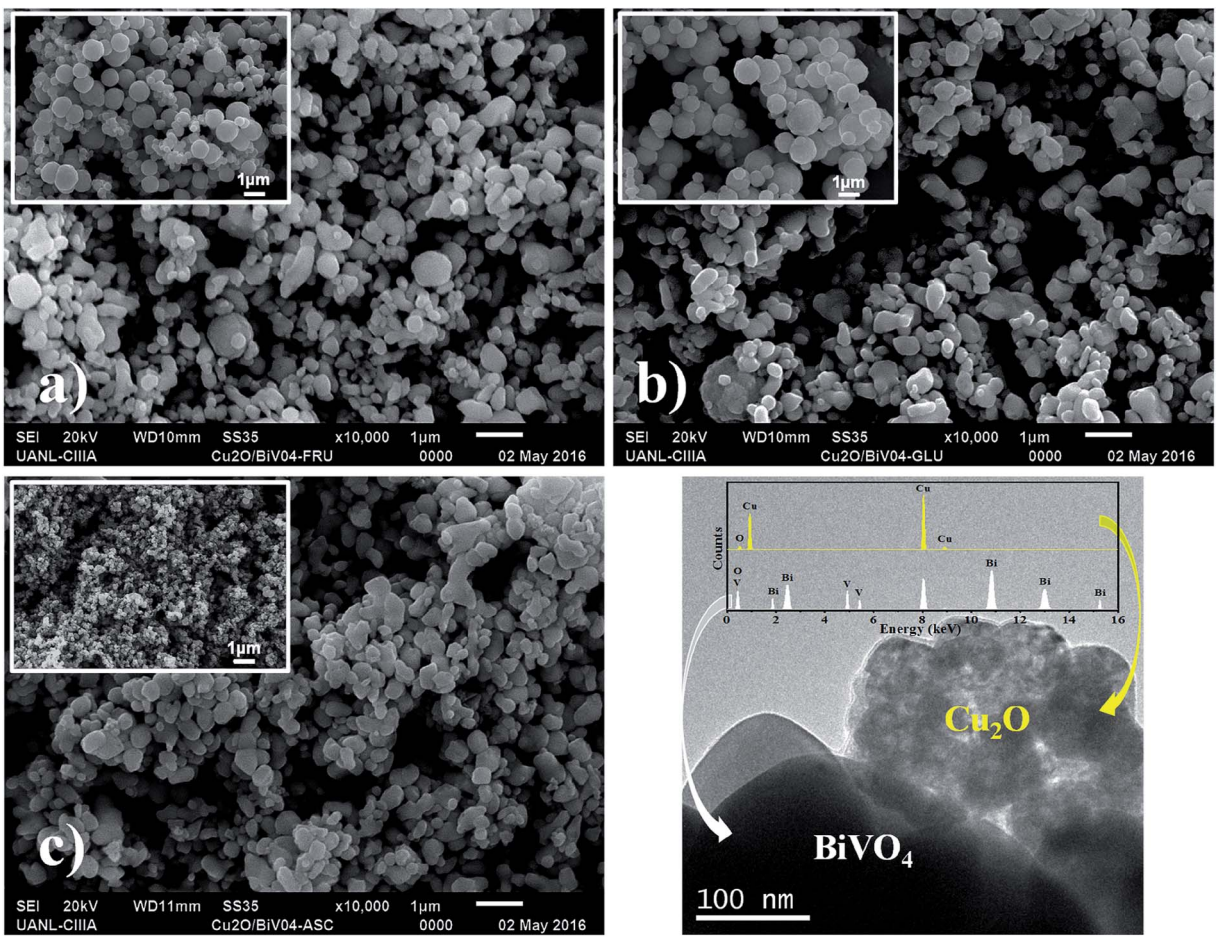

Fig. 2 SEM images of $Cu_2O/BiVO_4$ composites using different Cu_2O-co-catalyst; (a) $Cu_2O/BiVO_4$–F, (b) $Cu_2O/BiVO_4$–G and (c) $Cu_2O/BiVO_4$–A. (d) TEM image of $Cu_2O/BiVO_4$–A composite. The insets in (a–c) show corresponding images of pure Cu_2O particles. The inset in (d) shows the energy dispersive X-ray spectrum for the $Cu_2O/BiVO_4$–A composite.

The formation of a $Cu_2O/BiVO_4$ heterostructure was confirmed in the Cu_2O–A composite by TEM (Fig. 2d). This image revealed that $BiVO_4$ particles were covered by Cu_2O nanoparticles of *ca.* 50 nm, forming agglomerates. The elemental composition of $Cu_2O/BiVO_4$ was examined by energy-dispersive X-ray spectroscopy (inset Fig. 2d). Bi, V, Cu, O elements were all present in the $Cu_2O/BiVO_4$ composite photocatalyst.

3.4 DRS UV-vis results

The DRS UV-vis spectra indicate that all as-synthesized photocatalysts possessed strong absorption in UV and visible-light regions, as shown in Fig. S3 and S4 (ESI†). The results showed that Cu_2O samples exhibited absorption edges at 572, 650 and 652 nm for Cu_2O–A, Cu_2O–F and Cu_2O–G, respectively (Fig. S3†). A blue-shift in optical absorption edge is observed as particle size decreases. The band gap values were calculated by using Tauc plot,[33,34] and the obtained values were 2.36, 2.19 and 1.99 eV for Cu_2O–A, Cu_2O–F and Cu_2O–G, respectively. These results revealed that the reducing agent used in the synthesis process played an important role in the morphology and the optical properties of the as-synthesized Cu_2O, presumably, providing changes in the catalyst crystallinity which affects the bandgap.

The UV-vis spectra obtained for the composites showed a slight blue-shift from 515 to 510 nm with respect to pure $BiVO_4$ (516 nm), as shown in Fig. S4.† The band gap values of the composites were 2.49, 2.50 and 2.51 eV for $Cu_2O/BiVO_4$–A, $Cu_2O/BiVO_4$–F and $Cu_2O/BiVO_4$–G, respectively. The size of the band gap was mainly dominated by the optical features of $BiVO_4$, since the Cu_2O ratio present in the composite was only around 1%.

3.5 Electrochemical characterization

The flat-band potential of the composites was measured by electrochemical impedance spectroscopy. Fig. 3 shows the Mott–Schottky (M–S) plots for the pure $BiVO_4$ and composites films.

The M–S plots of the as-synthesized composites showed the presence of both positive and negative slopes, demonstrating the n-type and p-type electronic nature of the materials. These results confirm that the as-synthesized $Cu_2O/BiVO_4$ composites are heterostructured materials with a p–n junction, a feature that should enhance photogenerated charge separation and improve the photocatalytic activity.

It is well known that the slope of M–S plots is associated with the donor density of semiconductors.[35] The as-synthesized composites showed lower slopes in the Mott–Schottky plots compared to pure $BiVO_4$, indicating a higher donor density in the composites, and confirming that the heterojunction generates a lower charge recombination process.

The M–S plots also allow determination of E_{fb} by extrapolation of the positive and negative slope plots to the *x*-axis. The values for the positive slopes were −0.59, −0.57 and −0.36 V (*vs.* Ag/AgCl at pH 6.1), and for the negative slopes were −0.18, −0.30 and −0.04 V (*vs.* Ag/AgCl at pH 6.1) for $Cu_2O/BiVO_4$–A, $Cu_2O/BiVO_4$–F and $Cu_2O/BiVO_4$–G, respectively. The E_{fb} of pure $BiVO_4$ and Cu_2O–A films were also measured, as shown in Fig. 3 and S5,† resulting in −0.46 and −0.57 V (*vs.* Ag/AgCl at pH 6.1), respectively.

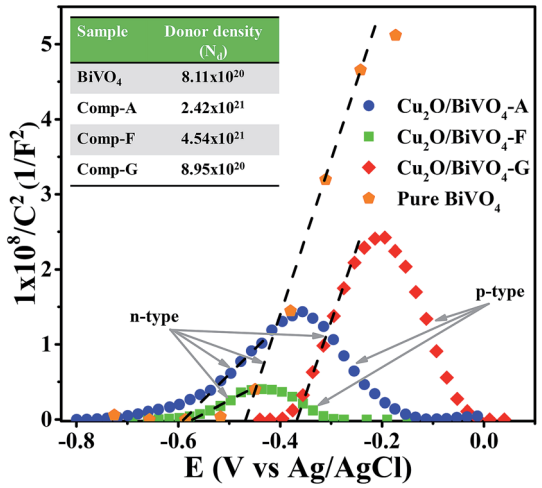

Fig. 3 Mott–Schottky plots of the pure $BiVO_4$ and composites-series. Inset shows the measured donor density (N_D) of each material.

Considering that the difference between the flat-band potential and the bottom edge of the conduction band or the top edge of the valence band is negligible for a n-type or p-type semiconductor, respectively,[36] the energy levels of the conduction band for pure $BiVO_4$ and the valence band for pure Cu_2O could be estimated, as described in Fig. 4.

Based on the flat-band potentials (or apparent Fermi levels) and the optical band gap energy values estimated above, it is possible to construct the potential energy diagram for all the as-synthesized samples, as illustrated in Fig. 4. According to the schematic diagram, before contact of materials, the conduction band of Cu_2O–G film is more positive than that of Cu_2O–A and Cu_2O–F films. When the two semiconductors are in contact, the conduction band of $Cu_2O/BiVO_4$–A and $Cu_2O/BiVO_4$–F composites powders are negatively shifted *ca.* 127 and 106 mV, respectively, with respect to that of $BiVO_4$, indicating that only in these composites it is possible the p–n junction formation and the injection of free electrons from $BiVO_4$ into Cu_2O, thus providing an enhanced charge-separation process. Meanwhile, in the $Cu_2O/BiVO_4$–G composite the valence band of Cu_2O is more negative than the conduction band of $BiVO_4$, thus the electron transfer is not possible.

3.6 Photocatalytic reactions

In order to investigate the influence of different Cu_2O co-catalyst on the photocatalytic activity of $BiVO_4$, the photoactivities of the as-synthesized $Cu_2O/BiVO_4$ composites were evaluated towards the degradation of 4-CP under visible-light irradiation, as shown in Fig. 5. The results show that the prepared $Cu_2O/BiVO_4$–A composite produced the best organic mineralization, 27% in 240 min, while the low activity of the

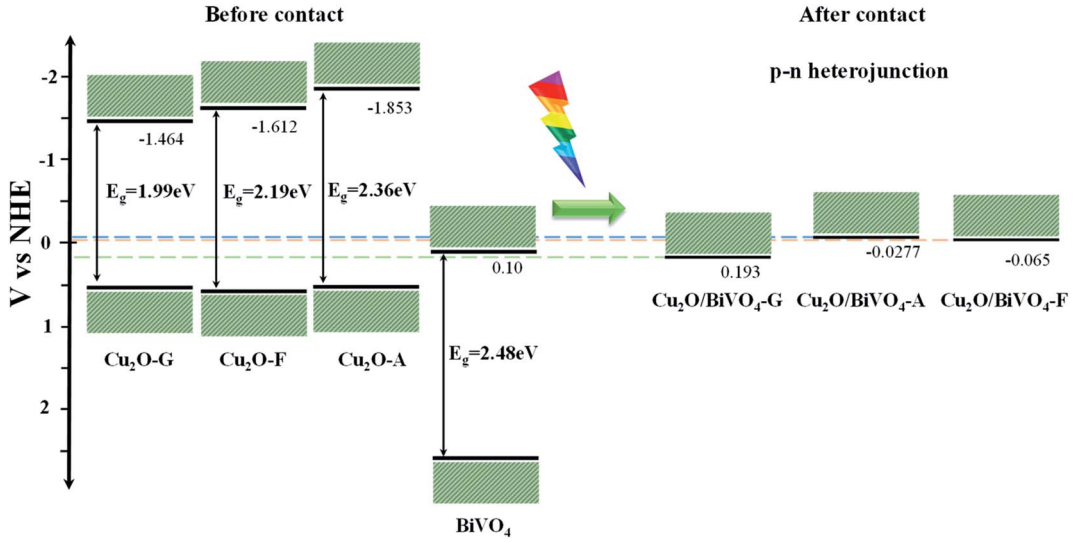

Fig. 4 Schematic diagram of the band energy of the as-synthesized Cu_2O-series, $BiVO_4$ and $Cu_2O/BiVO_4$ composites.

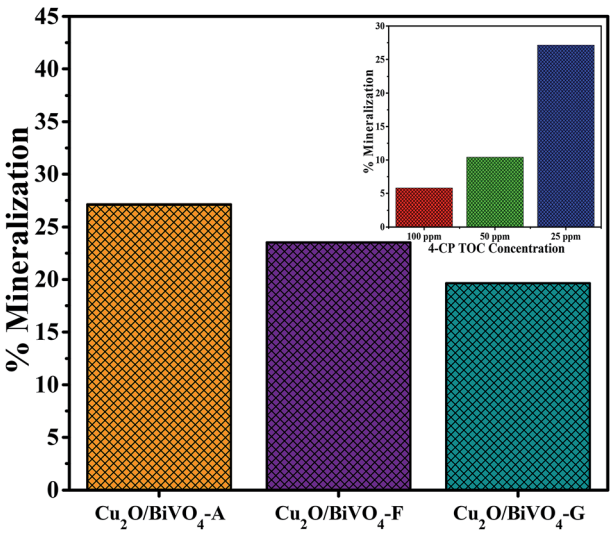

Fig. 5 Mineralization degree of 4-CP by $Cu_2O/BiVO_4$ composites with different Cu_2O co-catalysts under visible-light irradiation. Inset shows the effect of the initial 4-CP concentration on TOC removal during 4-CP removal using $Cu_2O/BiVO_4$–A catalyst under visible-light irradiation.

$Cu_2O/BiVO_4$–G photocatalyst was attributed to its minor charge density, as aforementioned.

The effect of 4-CP initial concentration on the mineralization degree was also studied (see inset of Fig. 5). The best photoactivity was observed at low 4-CP initial concentration. $Cu_2O/BiVO_4$–A composite reached *ca.* 27% mineralization degree at 50 ppm of 4-CP, while at higher concentrations of 100 and 200 ppm the mineralization degree was 10 and 5%, respectively. However, the removed amount was almost the same in terms of TOC measurement, indicating that, for the level of 4-CP concentrations herein studied, the surfaces of the three catalysts should be saturated, and their kinetic data do not depend on the 4-CP concentration, thus following similar reaction rates.

The effect of photocatalyst concentration was evaluated in order to improve the 4-CP photomineralization using $Cu_2O/BiVO_4$–A composite, using the following concentrations 1, 3 and 5 g L^{-1}, as illustrated in Fig. 6.

It is clear that the increase of the $Cu_2O/BiVO_4$–A loading in the reaction played an important role on the mineralization degree of 4-CP. The increase of the photocatalyst implies a major surface area where the organic molecule can be adsorbed, and a larger number of active sites. The best mineralization degree was 44% after 240 min with the 5 g L^{-1} concentration, whereas only 32% of mineralization was reached in the same time with the 3 g L^{-1} concentration.

Under the tested experimental conditions, the results indicate that the 4-CP photomineralization increases with catalyst

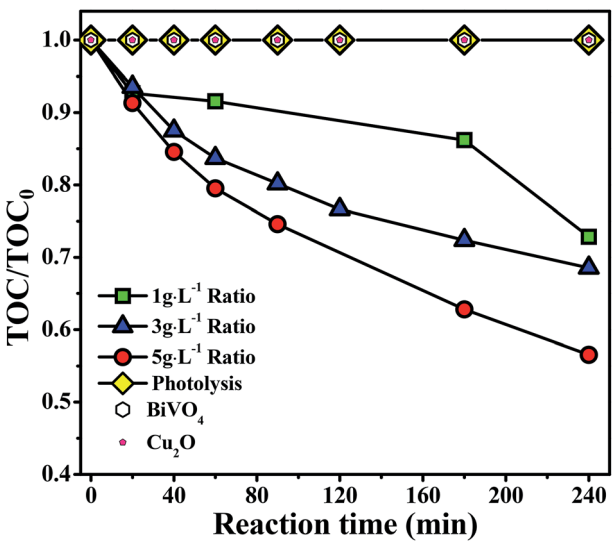

Fig. 6 Effect of the dosage of $Cu_2O/BiVO_4$ on TOC removal during 4-CP removal using $Cu_2O/BiVO_4$–A catalysts under visible-light irradiation.

loading, and no light scattering by the outer layers of catalyst in the reactor or any other screening effect are enough to negatively affect the photoactivity of $Cu_2O/BiVO_4$–A composite at high concentrations.

It is well know that $^{\bullet}OH$ and $^{\bullet}O_2^-$ radicals have an important role in the oxidation of organic molecules, and the addition of a permanent O_2 flux can significantly increase the number of radicals $^{\bullet}OH$ during the reaction.[37] Fig. 7 reveals that the mineralization degree of 4-CP rises to 76% after 240 min using $Cu_2O/BiVO_4$–A, in the presence of O_2 (flow of 250 mL h^{-1}) under visible-light irradiation. Thus, molecular oxygen is an electron scavenger assisting the stabilization of holes and enhancing the reaction rate.

The mineralization degree achieved in this work for 4-chlorophenol is better than that one reported in previous studies using visible-light-driven semiconductors materials such as N–TiO_2 (*ca.* 60% after 360 min), Eu_2O_3–TiO_2 (*ca.* 50% after 240 min), CuS (*ca.* 60% after 300 min), TiO_2/WO_3 (*ca.* 40% after 180 min).[38–41]

The visible-light photodegradation of 4-chlorophenol by $Cu_2O/BiVO_4$ composites can be achieved due to the improvement of the separation of photogenerated charge carriers on the composite. The proposed pathway for the photocatalytic degradation of 4-chlorophenol using $Cu_2O/BiVO_4$ composite is described with the following equations:

$$Cu_2O/BiVO_4 + h\nu \rightarrow BiVO_{4(h_{VB}^+)} + Cu_2O_{(e_{CB}^-)} \quad (9)$$

$$BiVO_{4(h_{VB}^+)} + {}^-OH \rightarrow {}^{\bullet}OH_{ads} + BiVO_4 \quad (10)$$

$$BiVO_{4(h_{VB}^+)} + \text{4-CP} \rightarrow\rightarrow \text{intermediates} \rightarrow\rightarrow \text{degraded products} + BiVO_4 \quad (11)$$

$$Cu_2O_{(e_{CB}^-)} + O_2 \rightarrow Cu_2O + {}^{\bullet}O_2^- \quad (12)$$

$$Cu_2O_{(e_{CB}^-)} + {}^{\bullet}O_2^- + H^+ \rightarrow Cu_2O + H_2O_2 \quad (13)$$

$$Cu_2O_{(e_{CB}^-)} + H_2O_2 \rightarrow {}^{\bullet}OH_{free} + {}^-OH + Cu_2O \quad (14)$$

$$\text{4-CP} + {}^{\bullet}OH_{free/ads} \rightarrow\rightarrow \text{4-CC} \rightarrow\rightarrow \text{HHQ} + \text{HBQ} \rightarrow\rightarrow \text{degraded products} \quad (15)$$

$$\text{HQ} + {}^{\bullet}OH_{free/ads} \rightarrow\rightarrow\rightarrow \text{intermediates} \rightarrow\rightarrow\rightarrow \text{degraded products} \quad (16)$$

$$\text{BQ} + {}^{\bullet}OH_{free/ads} \rightarrow\rightarrow\rightarrow \text{intermediates} \rightarrow\rightarrow\rightarrow \text{degraded products} \quad (17)$$

Once the charge carriers are photogenerated by visible-light (reaction (9)), the conduction band (CB) electrons of $BiVO_4$ are transferred to the valence band (VB) of Cu_2O resulting in the presence of free holes on the VB of $BiVO_4$ and free electrons on the CB of Cu_2O.

On other hand, the free holes on the VB of $BiVO_4$ react with 4-chlorophenol or hydroxide anion either free or adsorbed (reactions (10) and (11)), to produce the direct oxidation of organic molecules or the generation of $^{\bullet}OH$ radical, respectively. The free electrons on the CB of Cu_2O reduce the oxygen molecule resulting in the generation of $^{\bullet}OH$ radical by a series of reactions ((12)–(14)). Thus, the generation of $^{\bullet}OH$ radical is favored by the oxygen presence due to its role as electron scavenger. The oxidation reactions of 4-chlorophenol and intermediates, such as, hydroquinone (HQ) and benzoquinone (BQ), are carried out by the $^{\bullet}OH$ radical (reactions (15)–(17)) as reported in previous studies using different photocatalyst materials.[1,18]

In order to evaluate the reproducibility of the $Cu_2O/BiVO_4$ composite performance towards the 4-CP photomineralization, which is an important factor for applications related to water disinfection, reuse of the composite material was also investigated under visible-light irradiation (Fig. 8). After three cycles,

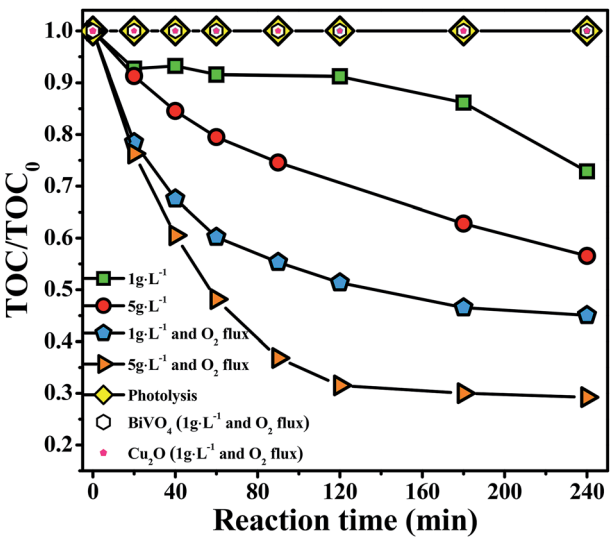

Fig. 7 Effect of continuous O_2 flux during the mineralization of 4-CP by $Cu_2O/BiVO_4$–A under visible-light irradiation and different photocatalyst dosage.

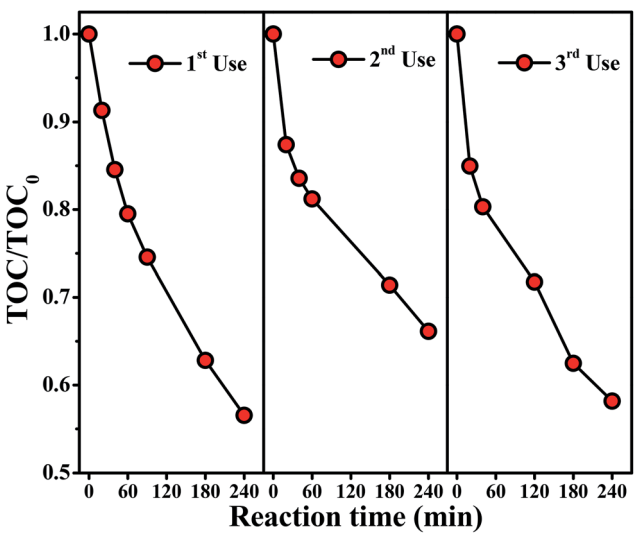

Fig. 8 Recycling uses of $Cu_2O/BiVO_4$–A for degrading 4-CP under visible-light irradiation, condition used: 25 mg L^{-1} of 4-CP initial concentration and 5 g L^{-1} of photocatalyst.

the photoactivity of the composite did not exhibit any remarkable loss, confirming that the composite is stable during the photocatalytic reaction studied. The chemical stability of $Cu_2O/BiVO_4$ composite was also confirmed by XRD (Fig. S6†), demonstrating that the monoclinic and cubic crystal structure of $BiVO_4$ and Cu_2O, respectively, remains unchanged. These results showed the feasibility of organic photocatalytic mineralization by using $Cu_2O/BiVO_4$ composite catalyst.

3.7 Identification of 4-CP intermediates

The photodegradation of 4-CP was conducted during 240 min to analyze the degradation capacity of the $Cu_2O/BiVO_4$ composites under visible-light irradiation. Fig. S7† shows the UV-vis spectrum of 4-CP at $t = 0$ min (red continuous line) under the experimental conditions proposed in the present study. As observed, a characteristic band is obtained at approximately 279 nm, which is typical for aqueous media.[42] When the photocatalytic treatment is conducted for 20 min, a remarkable decrease is registered for the main peak, suggesting the 4-CP degradation into intermediate compounds. Multiple photocatalytic studies have successfully reported the mineralization of 4-CP into CO_2, however, while some of those studies report the predominance of hydroquinone (HQ),[43–45] others identify the predominant formation of 4-chlorocatechol (4-CC),[46,47] without discussing the influence of catalyst or particular experimental condition favoring the formation of a determined intermediate.

Under this premise, the formation of any of these aromatic compounds was explored during the course of photocatalytic degradation (*i.e.* $t = 20$ min). Fig. 9 exhibits an UV-vis spectrum that was carried out to detect HQ in aqueous solution (50 mg L^{-1}). The single peak recorded at ~296 nm, which agrees with the literature,[48] is an indicator of the HQ presence. On the other hand, it was not possible to dissolve 4-CC in water in a concentration range detected by UV-vis spectroscopy, neither to find experimental data in literature concerning UV-vis spectrum for this aromatic compound.

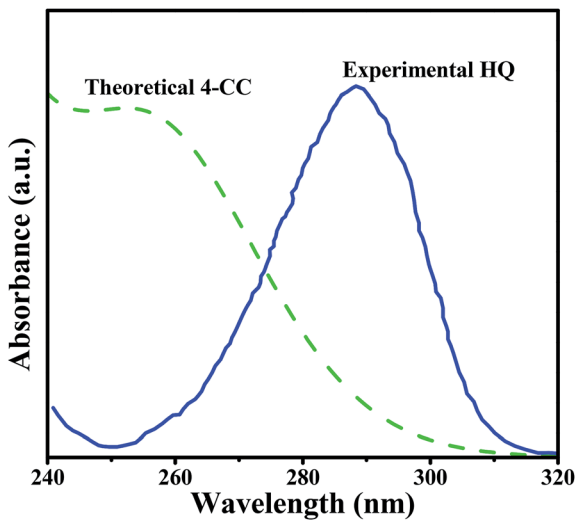

Fig. 9 Experimental UV-vis spectrum collected for standard hydroquinone (HQ, continuous line) in a 50 mg L^{-1} aqueous solution, and theoretical UV-vis spectrum computed for 4-chlorocatechol (4-CC, dashed line) using time-dependent density functional theory (B3LYP/6-311+g(d,p)).

The UV-vis spectrum of 4-CC was simulated (Fig. 9) using time-dependent density functional theory (TDDFT), in order to confront it against the data shown in Fig. S7.† As observed in this figure ($t = 20$ min), a small peak at 279 nm reveals the remaining 4-CP in solution, while the band at 253 nm can be assigned to the formation of 4-CC intermediate, as confirmed in the simulated spectrum described in Fig. 9. Note that this absorption band is located relatively far away from the HQ peak (296 nm, refer to Fig. 9),[48] which also precludes detection of *p*-benzoquinone (~244 nm).[49] Accordingly, 4-CC production is favored under the experimental conditions herein used. When the treatment reaches 40 min, the presence of 4-CP vanishes from the UV-vis spectrum (Fig. S7†) and only 4-CC is registered in the analysis, confirming the complete destruction of the original aromatic compound. Subsequently, abatement of 4-CC can be observed up to 240 min. It has been reported that the reaction mechanism for 4-CC degradation can involve the generation of malic, maleic and fumaric acids.[50] However, absorption bands at wavelengths higher than 320 nm, the typical absorption ranges for these compounds, were not detected. Another possibility is that these compounds could be present in concentrations lower than the detection limit of the spectrophotometer. A forthcoming study devoted to account for the reaction mechanism of 4-CP photomineralization with $Cu_2O/BiVO_4$ composite catalysts will involve detailed analysis of intermediates using high-performance liquid chromatography-mass spectrometry (HPLC-MS).

4. Conclusions

$Cu_2O/BiVO_4$ composites catalysts with different Cu_2O co-catalysts were synthesized by a simple impregnation method. The variation of the reducing reagent during the synthesis of Cu_2O played an important role in the optical, crystallographic and electrochemical properties of the $Cu_2O/BiVO_4$ composite catalyst, resulting in a different photocatalytic performance towards the mineralization of 4-CP in aqueous solutions under visible-light irradiation. The EIS study confirmed the p–n electronic behavior of the composites and demonstrated that a larger amount of charge carriers exist in $Cu_2O/BiVO_4$ composite catalyst with respect to the pure materials. The study of some experimental variables on the photocatalytic performance of $Cu_2O/BiVO_4$ catalysts, such as preparation method of co-catalyst, catalyst concentration, 4-CP initial concentration and oxygen flux showed their influence to enhance the photocatalytic activity of the material for 4-CP mineralization under visible-light irradiation. The complete destruction of 4-CP proceeded throughout the formation of 4-CC without involving the parallel generation of hydroquinone/*p*-benzoquinone, according to experimental and computed UV-vis spectra determined for pure intermediate compounds. From its performance and chemical stability and reusability, the $Cu_2O/BiVO_4$ composite

presented an evident potential for its use as catalyst for water remediation under visible-light irradiation.

Conflicts of interest

There are no conflicts to declare.

Acknowledgements

The authors acknowledge the financial support provided by the CONACYT (Grant No. 178895), the PAICYT, PRODEP, and the Spanish "Ministerio de Ciencia e Innovación", through project HIDROPILSOL (CTQ2013-47103-R). The authors thank Dr Felipe Montoya for a critical reading of the manuscript and for stimulating discussions.

References

1 J. Theurich, M. Lindner and D. W. Bahnemann, Photocatalytic degradation of 4-chlorophenol in aerated aqueous titanium dioxide suspensions: A kinetic and mechanistic study, *Langmuir*, 1996, **12**, 6368–6376.

2 M. Gomez, M. D. Murcia, N. Christofi, E. Gomez and J. L. Gomez, Photodegradation of 4-chlorophenol using XeBr, KrCl and Cl_2 barrier-discharge excilamps: A comparative study, *Chem. Eng. J.*, 2010, **158**, 120–128.

3 E. Pino and M. V. Encinas, Photocatalytic degradation of chlorophenols on TiO_2-325mesh and TiO_2-P25. An extended kinetic study of photodegradation under competitive conditions, *J. Photochem. Photobiol., A*, 2012, **242**, 20–27.

4 A. Fujishima and K. Honda, Electrochemical photolysis of water at a semiconductor electrode, *Nature*, 1972, **238**, 37–38.

5 A. Fujishima, X. Zhang and D. Tryk, TiO_2 photocatalysis and related surface phenomena, *Surf. Sci. Rep.*, 2008, **63**, 515–582.

6 A. Mills and J. Wang, Photomineralisation of 4-chlorophenol sensitised by TiO_2 thin films, *J. Photochem. Photobiol., A*, 1998, **118**, 53–63.

7 A. Mills and S. Morris, Photomineralization of 4-chlorophenol sensitized by titanium dioxide: A study of the initial kinetics of carbon dioxide photogeneration, *J. Photochem. Photobiol., A*, 1993, **71**, 75–83.

8 K. Villa, X. Domènech, U. M. García-Pérez and J. Peral, Optimization of the experimental conditions of hydrogen production by the Pt–(CdS/ZnS) system under visible light illumination, *RSC Adv.*, 2016, **6**, 36681–36688.

9 Y. Hsu, C. Yu, Y. Chen and Y. Lin, Fabrication of coral-like Cu_2O nanoelectrode for solar hydrogen generation, *J. Power Sources*, 2013, **242**, 541–547.

10 S. Kumar, C. M. A. Parlett, M. A. Isaacs, D. V. Jowett, R. E. Douthwaite, M. C. R. Cockett and A. F. Lee, Facile synthesis of hierarchical Cu_2O nanocubes as visible light photocatalysts, *Appl. Catal., B*, 2016, **189**, 226–232.

11 J. Liang, N. Kishi, T. Soga, T. Jimbo and M. Ahmed, Thin cuprous oxide films prepared by thermal oxidation of copper foils with water vapor, *Thin Solid Films*, 2012, **520**, 2679–2682.

12 Q. Zhu, Y. Zhang, J. Wang, F. Zhou and P. K. Chu, Microwave synthesis of cuprous oxide micro-/nanocrystals with different morphologies and photocatalytic activities, *J. Mater. Sci. Technol.*, 2011, **27**, 289–295.

13 Q. Zhu, Y. Zhang, F. Lv, P. K. Chu, Z. Ye and F. Zhou, Cuprous oxide created on sepiolite: Preparation, characterization, and photocatalytic activity in treatment of red water from 2,4,6-trinitrotoluene manufacturing, *J. Hazard. Mater.*, 2012, **217–218**, 11–18.

14 X. Zhang, J. Song, J. Jiao and X. Mei, Preparation and photocatalytic activity of cuprous oxides, *Solid State Sci.*, 2010, **12**, 1215–1219.

15 U. M. García Pérez, S. Sepúlveda-Guzmán, A. Martínez-de la Cruz and U. Ortiz Méndez, Photocatalytic activity of $BiVO_4$ nanospheres obtained by solution combustion synthesis using sodium carboxymethylcellulose, *J. Mol. Catal. A: Chem.*, 2011, **335**, 169–175.

16 X. Lin, Y. Wang, J. Zheng, C. Liu, Y. Yang and G. Che, Graphene quantum dot sensitized leaf-like $InVO_4/BiVO_4$ nanostructure: a novel ternary heterostructured QD-RGO/$InVO_4/BiVO_4$ composite with enhanced visible-light photocatalytic activity, *Dalton Trans.*, 2015, **44**, 19185–19193.

17 F. Guo, W. Shi, X. Lin, X. Yan, Y. Guo and G. Che, Novel $BiVO_4/InVO_4$ heterojunctions: Facile synthesis and efficient visible-light photocatalytic performance for the degradation of rhodamine B, *Sep. Purif. Technol.*, 2015, **141**, 246–255.

18 X. Lin, X. Guo, W. Shi, L. Zhao, Y. Yan and Q. Wang, Ternary heterostructured Ag–$BiVO_4/InVO_4$ composites: Synthesis and enhanced visible-light-driven photocatalytic activity, *J. Alloys Compd.*, 2015, **635**, 256–264.

19 L. Zhang and M. Jaroniec, Toward designing semiconductor-semiconductor heterojunctions for photocatalytic applications, *Appl. Surf. Sci.*, 2017, DOI: 10.1016/j.apsusc.2017.07.192.

20 X. Chen, S. Shen, L. Guo and S. S. Mao, Semiconductor-based Photocatalytic Hydrogen Generation, *Chem. Rev.*, 2010, **110**, 6503–6570.

21 S. Min, F. Wang, Z. Jin and J. Xu, Cu_2O nanoparticles decorated $BiVO_4$ as an effective visible-light-driven p–n heterojunction photocatalyst for methylene blue degradation, *Superlattices Microstruct.*, 2014, **74**, 294–307.

22 W. Wang, X. Huang, S. Wu, Y. Zhou, L. Wang, H. Shi, Y. Liang and B. Zou, Preparation of p–n junction $Cu_2O/BiVO_4$ heterogeneous nanostructures with enhanced visible-light photocatalytic activity, *Appl. Catal., B*, 2013, **134–135**, 293–301.

23 Q. Yuan, L. Chen, M. Xiong, J. He, S. Luo, C. Au and S. Yin, $Cu_2O/BiVO_4$ heterostructures: Synthesis and application in simultaneous photocatalytic oxidation of organic dyes and reduction of Cr (VI) under visible light, *Chem. Eng. J.*, 2014, **255**, 394–402.

24 E. Aguilera-Ruiz, U. M. García-Pérez, M. de la Garza-Galván, P. Zambrano-Robledo, B. Bermúdez-Reyes and J. Peral, Efficiency of $Cu_2O/BiVO_4$ particles prepared with a new soft

procedure on the degradation of dyes under visible-light irradiation, *Appl. Surf. Sci.*, 2015, **238**, 361–367.

25 H. Li, W. Hong, Y. Cui, X. Hu, S. Fan and L. Zhu, Enhancement of the visible light photocatalytic activity of $Cu_2O/BiVO_4$ catalysts synthesized by ultrasonic dispersion method at room temperature, *Mater. Sci. Eng., B*, 2014, **181**, 1–8.

26 U. M. García-Pérez, S. Sepúlveda-Guzmán and A. Martínez-de la Cruz, Nanostructured $BiVO_4$ photocatalysts synthesized via a polymer-assisted coprecipitation method and their photocatalytic properties under visible-light irradiation, *Solid State Sci.*, 2012, **14**, 293–298.

27 A. D. Becke, Density-functional thermochemistry. III. The role of exact exchange, *J. Chem. Phys.*, 1993, **98**, 5648–5652.

28 J. Tomasi, B. Mennucci and R. Cammi, Quantum mechanical continuum solvation models, *Chem. Rev.*, 2005, **105**, 2999–3093.

29 N. E. Markina, M. V. Pozharov and A. V. Markin, Synthesis of copper(I) oxide particles with variable color: Demonstrating size-dependent optical properties for high school students, *J. Chem. Educ.*, 2016, **93**, 704–707.

30 J. C. Speck, The Lobry De Bruyn-Alberda Van Ekenstein transformation, *Adv. Carbohydr. Chem.*, 1958, **13**, 63–103.

31 G. Jimenez-Cadena, E. Comini, M. Ferroni and G. Sberveglieri, Synthesis of Cu_2O bi-pyramids by reduction of $Cu(OH)_2$ in solution, *Mater. Lett.*, 2010, **64**, 469–471.

32 B. D. Cullity, *Elements of X-ray Diffraction*, Addison-Wesley, Massachusetts, 1987.

33 J. Tauc, Optical properties and electronic structure of amorphous Ge and Si, *Mater. Res. Bull.*, 1968, **3**, 37–46.

34 A. Ibrahim and S. K. J. Al-Ani, Models of optical absorption in amorphous semiconductors at the absorption edge - A review and re-evaluation, *Czech. J. Phys.*, 1994, **44**, 785–797.

35 K. Gelderman, L. Lee and S. W. Donne, Flat-band potential of a semiconductor: Using the Mott–Schottky equation, *J. Chem. Educ.*, 2007, **84**, 685–688.

36 J. Premkumar, Development of super-hydrophilicity on nitrogen-doped TiO_2 thin film surface by photoelectrochemical method under visible light, *Chem. Mater.*, 2004, **16**, 3980–3981.

37 S. Ahmed, M. G. Rasul, W. N. Martens, R. Brown and M. A. Hashib, Heterogeneous photocatalytic degradation of phenols in wastewater: A review on current status and developments, *Desalination*, 2010, **261**, 3–18.

38 H. Sun, Y. Bai, H. Liu, W. Jin and N. Xu, Photocatalytic decomposition of 4-chlorophenol over an efficient N-doped TiO_2 under sunlight irradiation, *J. Photochem. Photobiol., A*, 2009, **201**, 15–22.

39 M. Myilsamy, M. Mahalakshmi, N. Subha, A. Rajabhuvaneswari and V. Murugesan, Visible light responsive mesoporous graphene–Eu_2O_3/TiO_2 nanocomposites for the efficient photocatalytic degradation of 4-chlorophenol, *RSC Adv.*, 2016, **6**, 35024–35035.

40 S. Adhikari, D. Sarkar and G. Madras, Hierarchical Design of CuS Architectures for Visible Light Photocatalysis of 4-Chlorophenol, *ACS Omega*, 2017, **2**, 4009–4021.

41 C.-F. Lin, C.-H. Wu and Z.-N. Onn, Degradation of 4-chlorophenol in TiO_2, WO_3, SnO_2, TiO_2/WO_3 and TiO_2/SnO_2 systems, *J. Hazard. Mater.*, 2008, **154**, 1033–1039.

42 O. Thomas and C. Burgess, *UV spectrophotometry of water and wastewater, Techniques and Instrumentation in analytical chemistry*, Elsevier, Amsterdam, 2007.

43 H. Al-Ekabi, N. Serpone, E. Pelizzetti, C. Minero, M. A. Fox and R. B. Draper, Kinetic studies in heterogeneous photocatalysis. 2. titania-mediated degradation of 4-chlorophenol alone and in a three-component mixture of 4-chlorophenol, 2,4-dichlorophenol, and 2,4,5-thrichlorophenol in air-equilibrated aqueous media, *Langmuir*, 1989, **5**, 250–255.

44 G. Al-Sayyed, J. C. D'Oliveira and P. Pichat, Semiconductor-sensitized photodegradation of 4-chlorophenol in water, *J. Photochem. Photobiol., A*, 1991, **58**, 99–114.

45 H. C. Yatmaz, C. R. Howarth and C. Wallis in *Photocatalytic Purification and Treatment of Water and Air*, ed. D. F. Ollis and H. Al-Ekabi, Elsevier, Amsterdam, 1st edn, 1993, pp. 795–800.

46 A. Mills, S. Morris and R. Davies, Photomineralisation of 4-chlorophenol sensitised by titanium dioxide: a study of the intermediates, *J. Photochem. Photobiol., A*, 1993, **70**, 183–191.

47 T. Sehili, P. Boule and J. Lemaire, Photocatalysed transformation of chloroaromatic derivatives on zinc oxide III: Chlorophenols, *J. Photochem. Photobiol., A*, 1989, **50**, 117–127.

48 T. Wilke, M. Schneider and K. Kleinermanns, 1,4-hydroquinone is a hydrogen reservoir for fuel cells and recyclable via photocatalytic water splitting, *Open J. Phys. Chem.*, 2013, **3**, 97–102.

49 B. Boye, M. M. Dieng and E. Brillas, Degradation of herbicide 4-chlorophenoxyacetic acid by advanced electrochemical oxidation methods, *Environ. Sci. Technol.*, 2002, **36**, 3030–3035.

50 E. Brillas, A review on the degradation of organic pollutants in waters by UV photoelectro-Fenton and solar photoelectro-Fenton, *J. Braz. Chem. Soc.*, 2014, **25**, 393–417.